Journal Homepage: http://ijcpe.uobaghdad.edu.iq
Iraqi Journal of Chemical and Petroleum Engineering
Vol. 25 No. 2 (June 2024) 1 – 16
EISSN: 2618-0707, PISSN: 1997-4884

Investigating the Fouling Models of the Microfiltration Mixed Matrix Membranes-Based Oxide Nanoparticles Applied for Oil-in-Water Emulsion Separation

Sara A. Sadek [a], Sama M. Al-Jubouri [a], Sirhan Al-Batty [b, *]

a Department of Chemical Engineering, College of Engineering, University of Baghdad, Aljadria, Baghdad, Postcode: 10071, Iraq
b Department of Chemical & Process Engineering Technology, Jubail Industrial College, Jubail Industrial City, Postcode: 31961, Kingdom of Saudi Arabia

Abstract

Membrane fouling is a major problem encountered in the use of microfiltration (MF) processes to separate the emulsified oil from water. This work involves assessing the efficacy of removing oil-in-water emulsion (O/W emulsion), and evaluating fouling resistance by studying the membrane morphology before and after fouling, and after washing with different cleaning solutions via field emission scanning electron microscopy (FESEM) analysis. Also, the fundamental mechanism involved in the flux drop during crossflow MF has been assessed using models such as the Hermia blocking models and the modified model by Field. The standard and intermediate pore blocking models provided the best prediction for experimental behavior when analyzing the decay in the flux with time for the bio silicon oxide/polyvinylchloride (B-SiO_2/PVC) membrane and the stannic oxide/polyvinylchloride (SnO_2/PVC) membrane. This research established regression equations of the flux for both membranes in which these equations are highly correlated with R^2 of 98.33% for B-SiO_2/PVC and R^2 of 99.52% for SnO_2/PVC using the surface response methodology (RSM). The high flux recovery ratio (FRR) is indicative of the improved antifouling feature of the manufactured membranes where it was 96.8% for B-SiO_2/PVC and 94.6% for SnO_2/PVC. The results obtained by Hermia and Field were in good agreement with RSM analysis supporting the standard pore-blocking mechanism.

Keywords: Bio silicon oxide; polyvinylchloride; stannic oxide; fouling models; anti-fouling; microfiltration; oil-in-water emulsion.

Received on 13/01/2024, Received in Revised Form on 20/03/2024, Accepted on 20/03/2024, Published on 30/06/2024

https://doi.org/10.31699/IJCPE.2024.2.1

1- Introduction

The petroleum industry is a major contributor to pollution in the aquatic environment, primarily through the generation of oily wastewater emulsions containing concentrations ranging from 50 to 1000 mg/L [1]. Membrane separation technology, specifically ultrafiltration (UF) and microfiltration (MF) has acquired interest as an efficient method for eliminating dispersed oil droplets sized smaller than approximately 10 µm in emulsions [2, 3]. The petroleum industry uses crossflow MF to separate O/W emulsion, in which feed flows tangentially to the membrane or perpendicular to the permeate, unlike dead-end filtration. This configuration minimizes the accumulation of non-desirable species on the membrane, enabling a more rapid filtration process compared to the conventional dead-end filtration methods [4].

Membrane fouling is a major problem, particularly in the pressure-driven wastewater filtration process [5]. Fouling is caused by the feed water constituents coming into physical contact with the membrane. Membrane separation can be improved, and fouling can be reduced by maintaining the membrane clean. Therefore, it becomes of utmost necessity to have a reliable technique of cleaning for membrane separation procedures used in water purification. Membranes have been cleaned using either physical, chemical, or hybrid methods to remove the buildup of fouling and improve membrane performance as a whole [6].

Economically and technologically, MF of micro molecules imposes accurate modelling of fouling. It is widely acknowledged that there are four primary fouling mechanisms for MF membrane, as initially proposed by Hermia [7] and then updated by Field [8- 10]. The four types of blocking mechanisms are complete pore blocking, intermediate pore blocking, standard pore blocking, and cake layer formation as shown in Fig. 1. In both complete pore blocking and intermediate pore blocking, the particles possess identical dimensions to the membrane pores which comprehensively obstruct the entrances and impede the flow. However, during intermediate pore blocking, there is a buildup of some particles on top of previously deposited particles, narrowing the pore

*Corresponding Author: Email: batty_sa@jic.edu.sa

entrances. Standard pore blocking, in the meantime, leads to a reduction in membrane porosity and an increase in the membrane resistance due to the ability of tiny particles to adhere to the inner surface of the pores making them narrower and reducing the flow rate. Moreover, cake layer formation is the process in which larger particles gather on the membrane's surface forming a porous cake that is not completely impermeable but grows in thickness occasionally increasing the selectivity, and consequently raising the resistance of the membrane [11, 12].

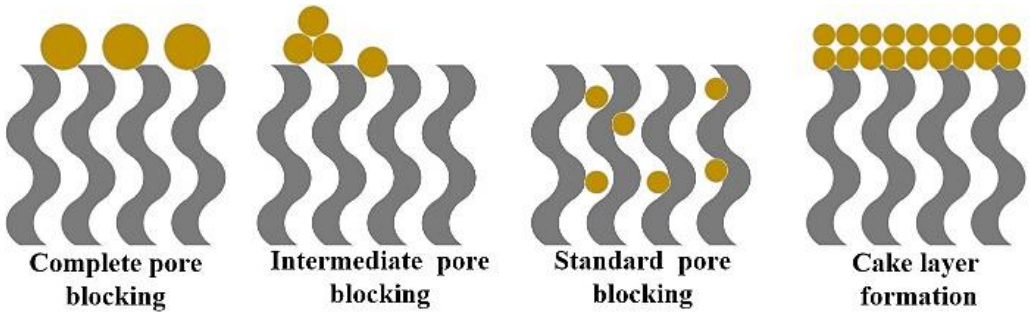

Fig. 1. Fouling Mechanisms

To address the issue of membrane fouling, various approaches were implemented to enhance the resistance to fouling and the hydrophilic properties of the polymeric membranes. These strategies encompass chemical and physical alterations of the membrane surface, as well as the incorporation of hydrophilic additives into the membrane matrix during the fabrication process [13- 18]. Synthetic and non-synthetic components have been incorporated with polymeric materials to form mixed matrix membranes (MMMs) to modify their chemical and physical properties. MMMs have opened unlimited new exploration opportunities due to their ability to minify the fouling of membranes during wastewater treatment applications and bypass the trade-off between permeability and selectivity. Polymer-inorganic MMMs are an exceptional fusion of the inorganic additives' distinctive characteristics, including anti-toxicity, mechanical and thermal resistance, and super-hydrophilicity, with the desirable features of the polymeric membranes [19-22]. Fouling can induce membrane surface degradation, resulting in a decrease in flow. Fouling can be decreased, and surface connectivity can be increased by integrating metal oxides with base membranes. SnO_2 is a well-known photocatalyst with excellent properties, which can be used to reduce fouling [14, 23-25]. B-SiO_2 has high hydrophilic properties so it can reduce fouling [13, 26, 27].

Response Surface Methodology (RSM) is a valuable quantitative technique for assessing the mathematical correlation between independent and dependent variables using a limited number of tests. The advantages of this approach are effective when numerous independent variables have an impact on multiple replies. Prediction of system behavior by the mathematical model that RSM provides, in a way enables effective decision-making and resource saving (e.g. time, money, and required experimental trial). The central composite design (CCD) is widely recognized as the most common and efficient strategy in RSM for statistically evaluating the interaction between independent factors and responses within the experimental range [28- 30].

The target of this work is finding a mathematical model that represents the fouling mechanism of the MMMs-based B-SiO_2 nanoparticles (NPs) and SnO_2 NPs prepared from the most hydrophobic polymer PVC that born to fouling, as well as studying the antifouling performance of these newly fabricated membranes. For the first time, the fouling performance and fouling mechanism will be investigated for the newly fabricated membranes using a crossflow pattern with the aid of different mathematical models. Furthermore, it aims to find empirical equations from the obtained experimental data to describe the flux variation with different operation variables such as feed concentrations, temperature, pressure, and time based on the response surface methodology (RSM) and analysis of variance (ANOVA).

2- Materials and Methodology

2.1. Martials and Fabrication Method

An O/W emulsion solution with a concentration of 100 mg/L was prepared as mentioned in the previous work [13, 14]. The size of the oil droplets in the feed solution was analyzed and the mean droplet size was 5.23 µm. Fabrication of the thin film MF membranes was conducted using PVC (grade 67 S) as a basic polymer provided by SABIC KSA. The solvent was DMAc ($CH_3CON(CH_3)_2$, 99.8 % assay) supplied by DASIT GROUP France. The surfactant was sodium dodecyl sulfate (SDS) ($C_{12}H_{25}NaO_4S$, 99.0 % assay) supplied by THOMAS BAKER Mumbai. The cleaning agent was ethylenediaminetetra acetic acid (EDTA) ($C_{10}H_{16}N_2O_8$ 98% assay) supplied by HIMEDIA, India. B-SiO_2 NPs were obtained from common water reeds (CWR) as mentioned in [13, 31, 32]. SnO_2 NPs with a particle size of 52.44 nm

(SnO_2, 99.5% assay) were supplied by MACKLIN, China. Two types of MMMs' were fabricated with a loading percentage of 0.5 wt.%, of B–SiO_2 NPs and 1 wt.% of SnO_2 NPs as shown in Table 1 and as explained in [13, 14].

Table 1. Compositions of Casting Solutions

Membrane Symbol	PVC wt.%	DMAc wt.%	B-SiO_2 NPs	SnO_2 NPs
S3	15	84.5	0.5	-
SN4	15	84	-	1

2.2. Antifouling Performance

Characterization before and after the fouling experiment was conducted using the field emission scanning electron microscope (FESEM) images to give important information about the morphology of the cross-section and top surfaces of the membranes. Cross-sectional membrane samples were obtained by previous freeze fracturing after immersion in liquid nitrogen. This test was conducted using the ZEISS model device. The membrane's roughness and pore size were determined using atomic force microscopy (AFM), Angstrom Advanced Inc., CSPM device. Fouling experiments for the S3 and SN4 membranes were conducted at a temperature of 25 ˚C and transmembrane pressure (TMP) of 1.5 bar as follows: PWF (J_o) (L/ m^2.h) of the S3 and SN4 membranes was initially measured for 1 h as previously explained in [13, 14]. After that, water was replaced by 100 mg/L O/W emulsion and the flux (J_1) (L/ m^2.h) was recorded for 1 h. Then, the fouled membrane sample was washed by soaking in 5 mM SDS cleaning solution for 45 min followed by distilled water (D.I.) for 30 min to rinse the chemical detergent (i.e., SDS). Washing procedures were repeated using 5 mM EDTA as a cleaning solution. Finally, the PWF (J_2) was measured again for 1 h. The flux recovery ratio (FRR%) was calculated using Eq.1, the relative flux reduction (RFR%) was calculated using Eq. 2, the reversible fouling ratio (R_r%) was calculated using Eq. 3, and the irreversible fouling ratio (R_{ir}%) was calculated using Eq. 4 [33, 34]:

$$FRR\% = \frac{J_2}{J_o} \times 100 \quad (1)$$

$$RFR\% = \left(1 - \frac{J_1}{J_o}\right) \times 100 \quad (2)$$

$$R_r\% = \left(\frac{J_2 - J_1}{J_o}\right) \times 100 \quad (3)$$

$$R_{ir}\% = \left(\frac{J_o - J_2}{J_o}\right) \times 100 \quad (4)$$

The membrane rejection percentage (R%) was calculated as given in the previous study [13, 14].

3- Membrane Fouling Models

Both types of fabricated membranes (S3 and SN4) were tested by the MF technique and their time-permeate flux (J) relationships were modeled. Across the MF time, the permeate volume declined as time progressed. The fouling mechanism during MF has been studied using the empirical models established by Hermia [7] and recently adapted for crossflow filtration by Field et al., [8] to characterize the decline of permeate flux.

3.1. Hermia Models

Hermia models were used for constant pressure dead-end filtration and the initial stage of crossflow operation [34]. The form of fouling depends on the value of n appearing in Eq. 5 [35- 38].

$$\frac{d^2t}{dv^2} = k\left(\frac{dt}{dv}\right)^n \quad (5)$$

For complete pore blocking, n is typically 2. For standard pore blocking, n is typically 3/2. For intermediate pore blocking, n is typically 1. For cake layer formation, n is typically 0. The factors examined by these models possess physical significance and aid in understanding the processes involved in membrane fouling [39]. The integrated form of Eq. 5 can be written in terms of permeate flux [40] as follows:

a) Complete pore blocking

$$\ln J = \ln J_O - K_B\, t \quad (6)$$

b) Standard pore blocking

$$J^{-0.5} = {J_0}^{-0.5} + K_S\, t \quad (7)$$

c) Intermediate pore blocking

$$J^{-1} = {J_0}^{-1} + K_I\, t \quad (8)$$

d) Cake layer formation

$$J^{-2} = {J_0}^{-2} + K_C\, t \quad (9)$$

The relationship between ln(J) and t, $J^{-0.5}$ and t, J^{-1} and t, and J^{-2} and t must exhibit a linear pattern. The slope of these lines corresponds to the values of K_B, K_S, K_I, and K_C, while the y-intercepts represent ln (J_o), $J_o^{-0.5}$, J_o^{-1}, and J_o^{-2} values, respectively. The model that accurately represents the experimental data, with a high correlation coefficient (R^2) value, i.e. close to 1, indicates the relevant fouling mechanism during crossflow MF [1, 41 -43].

3.2. Field Models

These models were modified depending on the above-mentioned Hermia models to analyze the fouling mechanisms of the membrane surface, resulting in a general differential given by Eq. 10.

$$-\frac{dJ}{dt} = K\,(J - J_{SS})J^{2-n} \quad (10)$$

The integrated form of Eq.10 can be written in the form of permeate flux, as shown in Eq. 11 to Eq. 13 [39, 9, 44].

a) Complete pore blocking

$$J = J_{SS} + (J_0 - J_{SS})e^{-K_B J_0 t} \quad (11)$$

b) Standard pore blocking

$$J^{-0.5} = J_0{}^{-0.5} + K_S\,t \quad (7)$$

c) Intermediate pore blocking

$$J = \frac{J_0 J_{SS} e^{K_I J_{SS} t}}{J_{SS} + J_0\left(e^{K_I J_{SS} t} - 1\right)} \quad (12)$$

d) Cake layer formation

$$t = \frac{1}{K_C\,J_{SS}{}^2}\ln\left[\left(\frac{J(J_0 - J_{SS})}{J_0(J - J_{SS})}\right) - J_{SS}\left(\frac{1}{J} - \frac{1}{J_0}\right)\right] \quad (13)$$

The linear relationships between time and the parameters of the complete pore-blocking model (Ln $[(J\text{-}J_{SS})/(J_0\text{-}J_{SS})]$), the standard pore-blocking model ($1/J^{0.5}$), the intermediated pore-blocking model (Ln $[J(J_0\text{-}J_{SS})/J_0(J\text{-}J_{SS})]$), and the cake layer formation model ($\ln[\left[\left(\frac{J(J_0-J_{SS})}{J_0(J-J_{SS})}\right) - J_{SS}\left(\frac{1}{J}-\frac{1}{J_0}\right)\right]]$) symbolled by (H), were established to calculate the constants (K_B, K_S, K_I, and K_C) in each relevant model. The model that accurately represents the experimental data, with a high R^2 value, i.e. close to 1, indicates the relevant fouling mechanism during crossflow MF.

4- Results and Discussion

4.1. Antifouling Measurements and Performance

Fig. 2 shows the flux obtained from S3 and SN4 membranes where they were cleaned using different washing solutions of 5 mM SDS and 5 mM EDTA at a feed sequence of D.I. followed by 100 mg/L O/W emulsion. The water flux of the membranes reduced to a significantly low level throughout the filtration process when the feed was changed from pure water to an O/W emulsion. This could be ascribed to the presence of oil in the emulsion. The values of FRR% for the S3 and SN4 membranes cleaned by SDS were 96.838% and 94.663%. However, these values were 92.885% and 90.730% when cleaned by EDTA. The high FRR% denotes the improved antifouling property of the fabricated membrane.

The improved antifouling performance was because of the smooth top surface as shown by the AFM results presented in [13, 14], which prevented the oil droplets from being captured by the surface features. SDS proved to be a superior cleanser in comparison to EDTA. SDS has a powerful cleaning effect due to its ability to change the interfacial tension of water. SDS achieves efficient cleaning because it combines hydrophobic and hydrophilic groups. Surfactants possess the power to form micelles around macromolecules to enhance their solubility and facilitate the elimination of the precipitated compounds from the surface of the membrane. Generally, SDS has superior solvency for oil and grease, but EDTA is particularly efficient in removing deposited minerals from membranes. Furthermore, studies have demonstrated that EDTA enhanced the effectiveness of cleaning fouled membranes by eliminating divalent cations from intricate organic compounds [6, 45, 46]. EDTA structure has six bonding points. EDTA strongly combines with calcium and dispersal minerals and can interact with these foulants and remove them from the membrane surface [47].

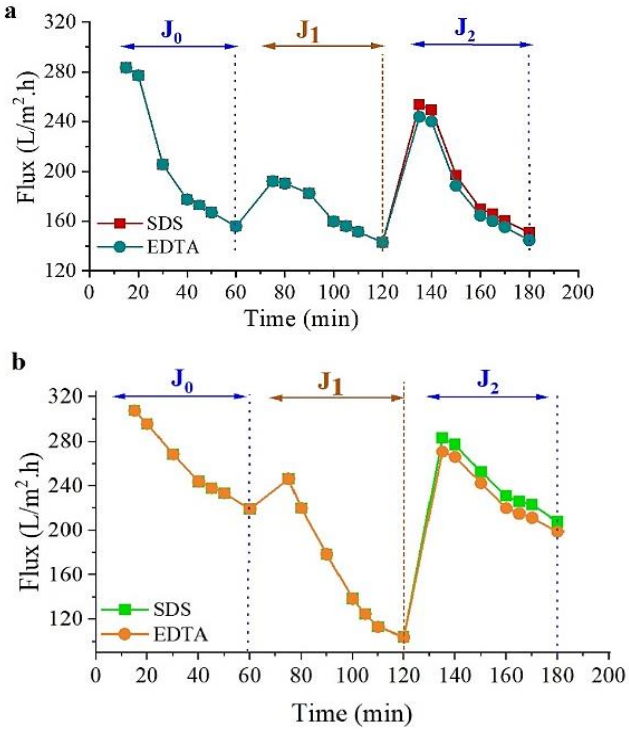

Fig. 2. Flux Variation of (a) S3 Membrane (b) SN4 Membrane at 25 ˚C and 1.5 bar

Table 2 shows the antifouling performance of S3 and SN4 membranes. The RFR% of the SN4 membrane was higher than that of the S3 membrane because the mean pore size (d_a) of the SN4 membrane was smaller than that of S3 due to the high casting solution viscosity as previously reported in [13, 14]. Where the membrane with small pore size showed difficulty in cleaning by chemicals only. The FRR% was high using both cleaning solutions. The adhesion affinity of oil increased inside the internal membrane pores resulting in obstructing the permeated passage. Because SN4's average surface roughness (R_a) was higher than that of S3, so smoother surfaces showed the best antifouling performance [27, 48].

Table 2. Fouling Performance of S3 and SN4 Membranes at 25 °C and 1.5 bar

Membrane	Cleaning solution	R%	FRR %	RFR%	R_r%	R_{ir}%
S3	SDS	98.15	96.838	8.300	5.138	3.162
	EDTA	98.3	92.885	8.300	1.186	7.115
SN4	SDS	99.3	94.663	52.528	47.191	5.337
	EDTA	99.5	90.730	52.528	43.258	9.270

AFM results of both membranes are shown in Fig. 3 represented by the R_a and d_a. Incorporating nano additives resulted in an improvement in the antifouling properties. The low value of RFR% and the high value of FRR% indicate enhanced membrane antifouling for both membranes. These results agreed with other studies conducted by Kazemi et al., [49]. The PWF declined after washing; since removing all oil drops from the membrane texture was impossible and some pollutants were retained in the membrane structure. The R% of the S3 was 98.15% and 99.3% for SN4. This can be explained as the oil drops accumulated on the S3 and SN4 membrane surfaces during filtration causing pore filling with oil as time proceeded which formed an oil layer on the membrane surface acting as an additional resistance for oil passage through the membrane and thereby gave high R%.

Membrane fouling can be either reversible or irreversible. In reversible fouling, oil can be physically washed away because the bonds are weaker. But in irreversible fouling, chemical washing is needed to remove the oil which may damage the membranes and make them last less. The R_{ir}% for S3 was 3.15% and 7.11%, while it was 5.33% and 9.27% for SN4 using SDS and EDTA cleaning solutions, respectively. Obtaining R_{ir}% values less than 10% indicates conducting an effective cleaning using the mentioned solutions which allowed easy removal of oil drops present on the membrane surface. Also, the results indicate promising enhancement in the antifouling performance. These results agree with those obtained by Geleta et al. [50].

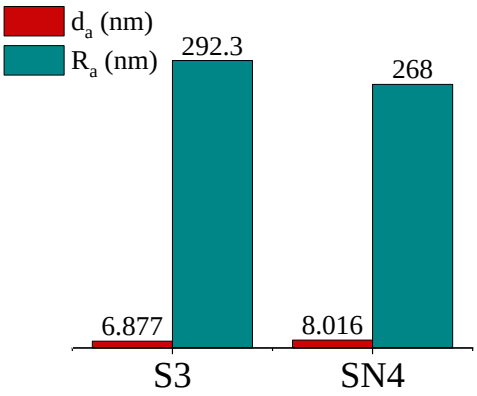

Fig. 3. AFM Results

In this study, only chemical cleaning was performed without using any physical or hydrodynamic action. Using chemical cleansing agents can degrade the structural stability of the fouling layers by reacting with the foulants. The absence of the action of physical cleaning was clear and approved through obtaining R_r% larger than R_{ir}% in both fabricated membranes which is the main cause of the flux decline. The R_r% of SN4 was 47.19% and it was higher than that of S3 which was 5.13% because SN4 has a rougher surface with more bends which increases the number of potential places to break oil droplets during the filtration process. The partial obstruction occurred because the broken tiny oil drops can easily penetrate the membrane pore. Ultimately, the RFR% was low for both membranes because adding B-SiO_2 NPs and SnO_2 NPs highly improved the properties of these membranes, especially the hydrophilicity as reported in the previous work [13, 14]. These studies pointed out that adding hydrophilic functional groups to the composite membrane can improve the hydrogen bonding with the molecules of water, reduce the hydrophobic interactions, and increase the resistance to fouling.

Fig. 4 and Fig. 5 show FESEM images of the top surface and the cross-section of S3 and SN4 membranes before and after foulant washing. The S3 and SN4 treated with SDS showed small amounts of adsorbed impurities on the top surface and no visible signs referring to degradation of the top surface as shown in Fig. 4 b and Fig. 5 b. The membranes treated with EDTA showed the presence of creases on the skin surface which likely formed during the drying of the sample as shown in Fig. 4 c and Fig. 5 c. More contamination appeared when using EDTA than when using SDS as a cleaning solution. The cross-section of the S3 and SN4 membranes cleaned by SDS and EDTA showed a slight increase in the size of cavities while the micropores remained at the same density. Also, some dark spots appeared in the membrane cavities which revealed the deposition of the oil droplets in these pores that cannot be easily removed by simple chemical washing, and they may need physical action. Since the hydrodynamic conditions are required to promote contact between the SDS and EDTA with the oil droplets, for these reasons, restoring the first permeability of 100% is not possible.

Following the removal of the predominantly negatively charged oil fouling using the SDS washing solution, a residual presence of anionic surfactant molecules (i.e., SDS) may persist on the membrane surface, hence enhancing the repulsive forces against the O/W emulsion. SDS has hydrophobic groups that adsorb oil and hydrophilic groups that adsorb water; subsequently, the presence of SDS will improve the hydrophilic property of the

fabricated membranes and the cleaned membrane with superior antifouling will result. For these reasons, SDS gives favorable washing performance [51].

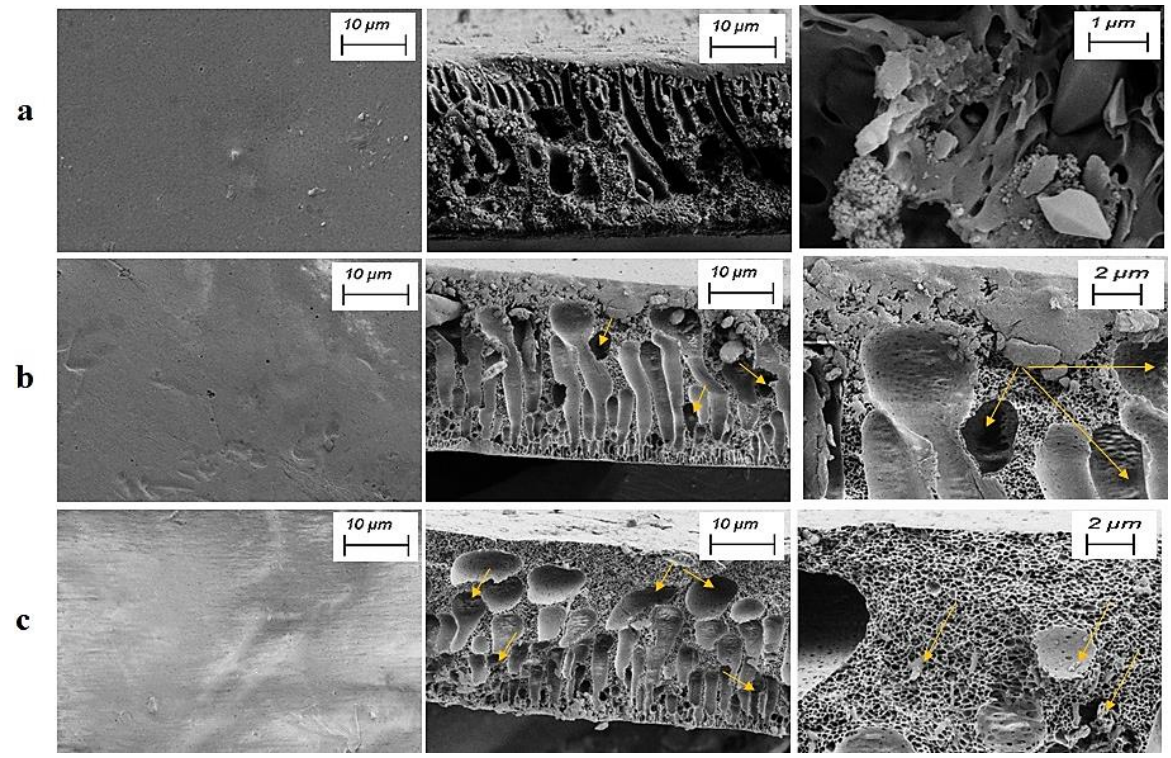

Fig. 4. FESEM Images of the Surface and Cross-Section of the S3 Membrane (from the Right to the Left). Where (a) Membranes Before Fouling (b) Membranes After Washing with SDS (c) Membranes After Washing with EDTA

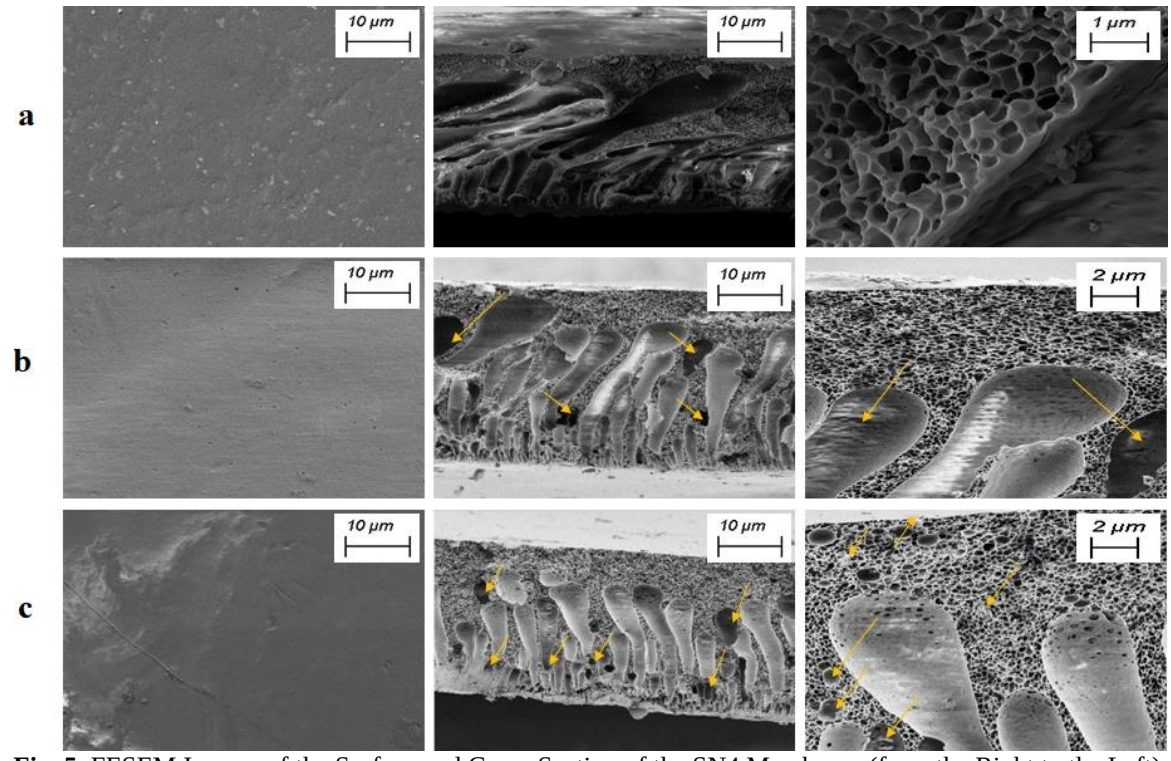

Fig. 5. FESEM Images of the Surface and Cross-Section of the SN4 Membrane (from the Right to the Left). Where (a) Membranes Before Fouling (b) Membranes After Washing with SDS (c) Membranes After Washing with EDTA

4.2. Applying the Fouling Models

The Hermia's and Field fouling models were applied to the data obtained from studying the O/W emulsion filtration to find out the fouling mechanism of S3 and SN4 membranes. Fig. 6 to Fig. 9 show the plots of Hermia's and Field models. Table 3 displays the values of the fitting parameters and equations for S3 and SN4 membranes obtained using the Hermia and Field models. Fig. 6 shows that the standard pore-blocking model was the best mechanism for describing S3 membrane fouling with a high R^2 value of 0.9686. The complete pore-blocking model also showed acceptable agreement with the experimental permeation flux data with an R^2 value of 0.968. The S3 membrane suffered from the deposition of oil droplets on the membrane pores due to the adsorption mechanism. To obtain the desirable antifouling performance of membranes, it is recommended to use physical methods like back washing, water flushing, and ultrasonication instead of using chemical agents only.

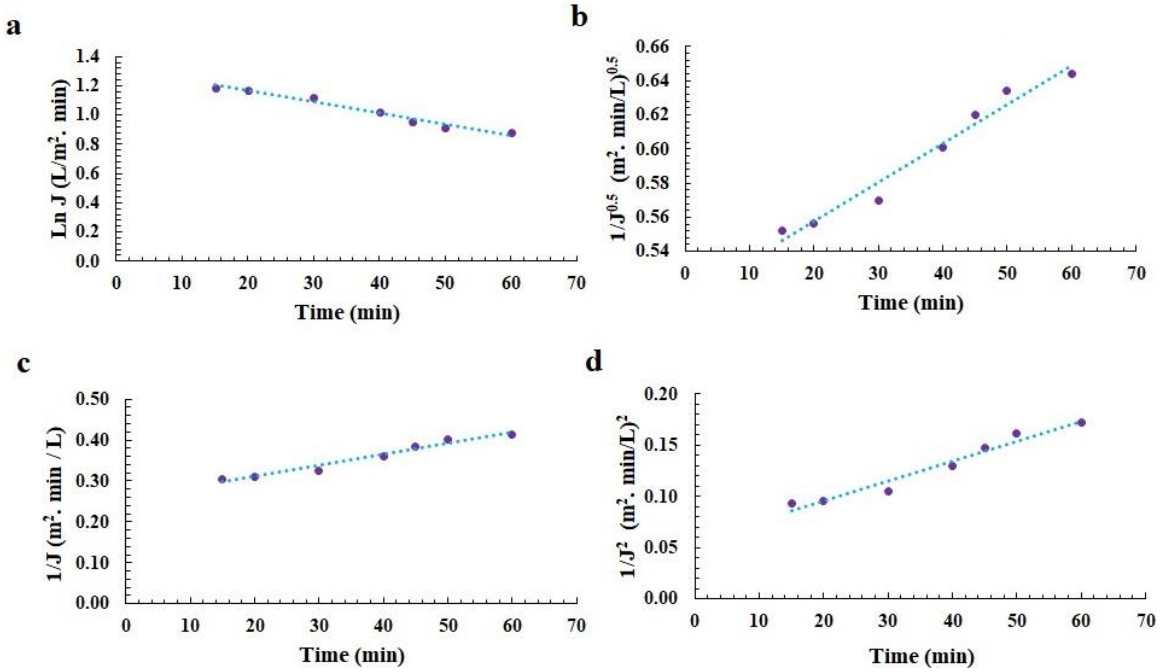

Fig. 6. The Plots of the Hermia Model for the S3 Membrane (a) Complet Pore Blocking Model, (b) Standard Pore Blocking Model, (c) Intermediate Pore Blocking Model, and (d) Cake Layer Formation Model

Fig. 8 shows the modified Field model applied on S3 revealing that the standard pore-blocking model was the controlling fouling mechanism with a high R^2 value of 0.9686 followed by complete pore blocking with an R^2 value of 0.7359. Eq. 7 represents the standard pore blocking model for both Hermia and Field. This model was the controlling fouling mechanism for the S3 membrane during filtration of O/W emulsion. If the membrane pores are assumed to have a fixed length and radius, the accumulation of oil on the pore inside walls would reduce the pore volume. As fouling is caused by the internal pore blocking, there is no backward transfer of oil molecules from the internal pores of the S3 membrane to the bulk feed solution and the hydrodynamic action of the crossflow is diminished [47, 39, 9].

Fig. 7 shows the fouling mechanism of the SN4 membrane studied using the Hermia model. The intermediate pore blocking mechanism with R^2 of 0.9898 was the best fouling model elucidating the fouling mechanism followed by standard pore blocking with R^2 of 0.988. When the Filed model was applied (see Fig. 9), the standard pore blocking gave the highest R^2 of 0.988. Where Field developed the Hermia fouling model based on the assumption that the hydrodynamic action during crossflow MF leads to preventing the oil drops from accumulating on the membrane surface and returning oil to the feed stream. Therefore, after a long time of filtration operation, the flux arrives at a steady state value symbolled by J_{ss} which appears in its modified model (i.e., Eq. 11 to Eq. 13) [10, 8]. The standard pore-blocking model is mostly irreversible and can be cleaned using a suitable surfactant or chemical agent. Therefore, this model was the best model describing the results of the fouling performance experiment which showed a low value of R_{ir}% for both membranes after performing excellent chemical washing procedures.

A comparison of filtration models predicted by Hermia and Field with experimental data of S3 and SN4 membranes is displayed in Fig. 10 and Fig. 11, respectively. The S3 membrane showed excellent fitted data with the standard blocking model when applying the Hermia and Field models. While the SN4 membrane fitted with the intermediate pore blocking when applying the Hermia model and the

standard pore blocking when applying the Field model. Fig. 10 and Fig. 11 b do not show the curves representing the fitting with the cake layer formation model because this model represented by Eq. 13 which was developed by Field cannot be applicable to predicate the theoretical approach with these experimental data for both S3 and SN4 membranes. This is because the fouling mechanism was studied at 25 ˚C, constant TMP of 1.5 bar, and 100 mg/L of feed concentration which represents the initial stage of flux decline using crossflow configuration, and these conditions do not allow the formation of a cake layer. The hydrodynamic action of crossflow filtration affects the fouling mechanism and prevents cake layer formation. As a result, the Hermia model was the best to describe the fouling mechanism in these initial stages [44, 52, 53]. So far, there is a limited understanding of the impacts of the fundamental factors that contribute to membrane fouling. Additionally, there is no comprehensive theoretical framework for membrane fouling that can effectively explain the process of membrane fouling [51].

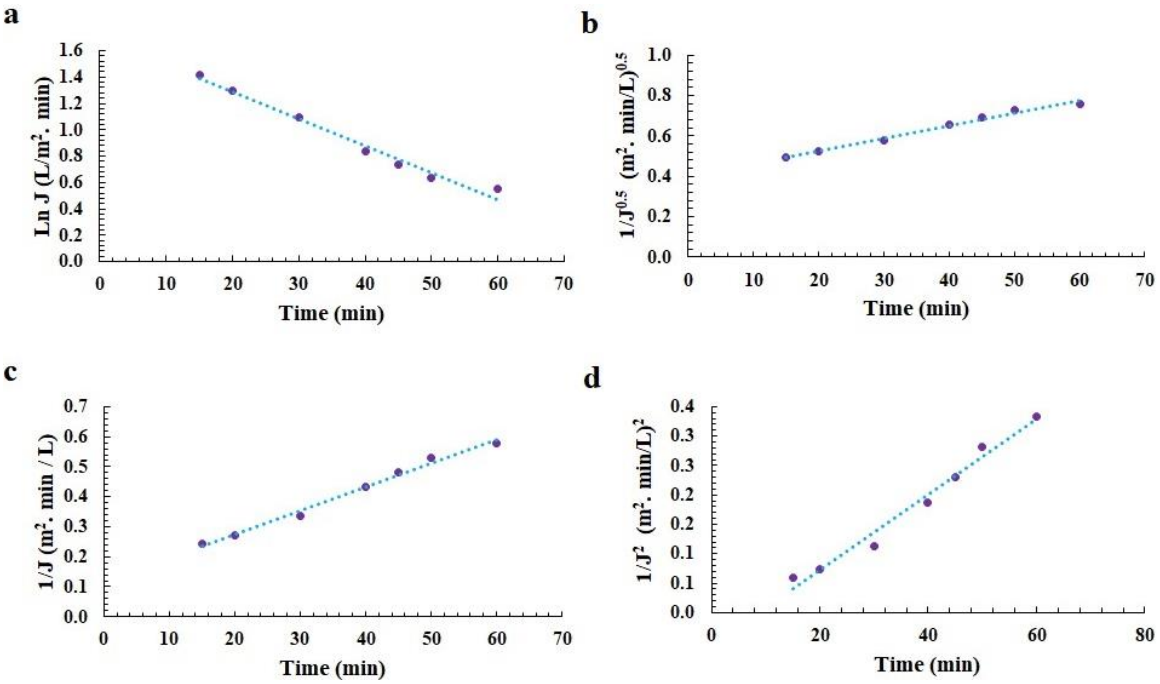

Fig. 7. The Plots of the Hermia Model for the SN4 Membrane (a) Complet Pore Blocking Model, (b) Standard Pore Blocking Model, (c) Intermediate Pore Blocking Model, and (d) Cake Layer Formation Model

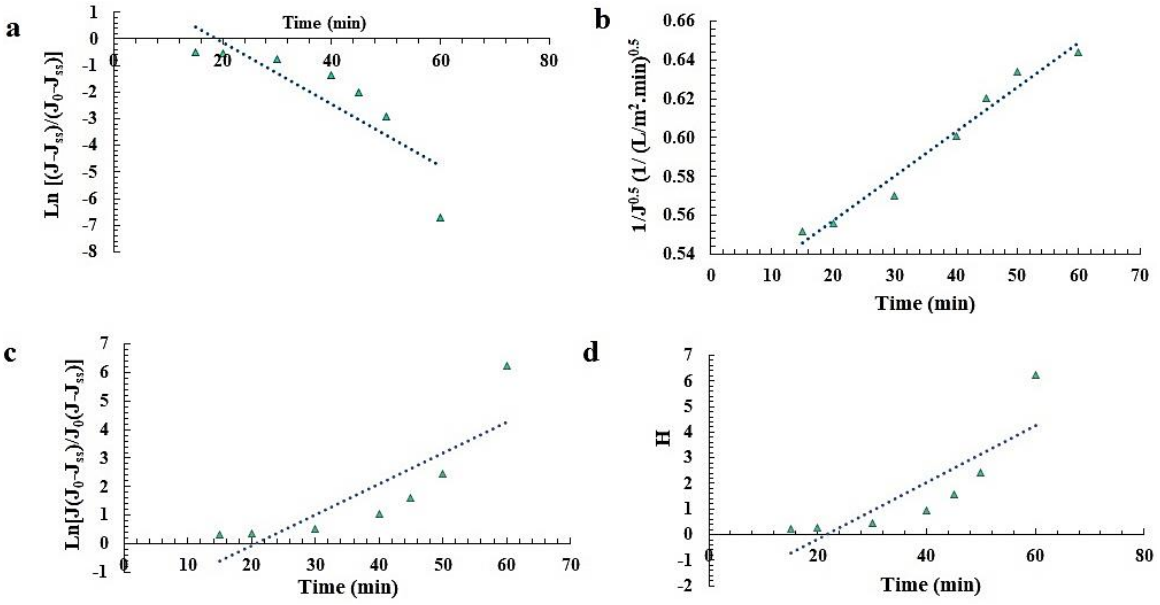

Fig. 8. The Plots of the Modified Field Model for the S3 Membrane (a) Complet Pore Blocking Model, (b) Standard Pore Blocking Model, (c) Intermediate Pore Blocking Model, and (d) Cake Layer Formation Model

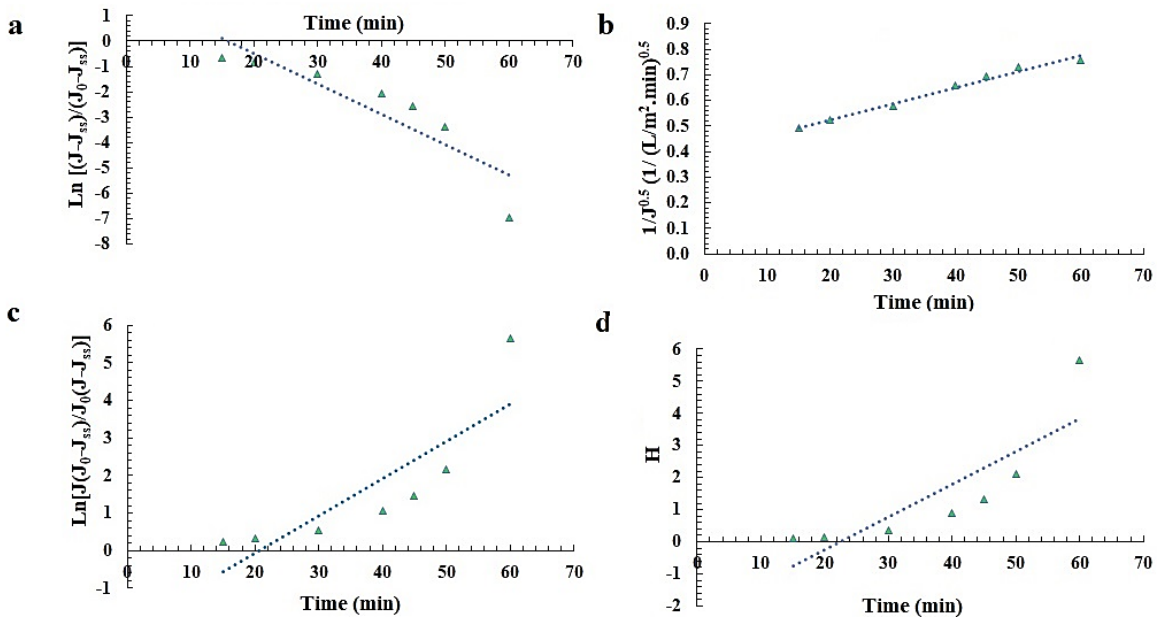

Fig. 9. The Plots of the Modified Field Model for the SN4 Membrane (a) Complet Pore Blocking Model, (b) Standard Pore Blocking Model, (c) Intermediate Pore Blocking Model, and (d) Cake Layer Formation Model

Table 3. The Determined Parameters of the Fouling Models

Models	Fitting parameters	Hermia Membrane		Field Membrane	
		S3	SN4	S3	SN4
Complete pore-blocking	K_B (m^2/L)	0.0077	0.0204	0.0305	0.0191
	R^2	0.968	0.9813	0.7359	0.8008
	Fitting Equations	y = -0.0077x + 1.3211	y = -0.0204x + 1.6929	y = -0.1162x + 2.2113	y = -0.1192x + 1.8973
Standard pore-blocking	K_S (m/ $L^{0.5}$. $min^{0.5}$)	0.0023	0.0063	0.0023	0.0063
	R^2	0.9686	0.988	0.9686	0.988
	Fitting Equations	y = 0.0023x + 0.5119	y = 0.0063x + 0.3998	y = 0.0023x + 0.5119	y = 0.0063x + 0.3998
Intermediate pore-blocking	K_I (m^2/L)	0.0027	0.0079	0.0449	0.0572
	R^2	0.9673	0.9898	0.7042	0.7166
	Fitting Equations	y = 0.0027x + 0.2562	y = 0.0079x + 0.118	y = 0.1084x - 2.2275	y = 0.0989x - 2.0379
Cake layer formation	K_C (m^4.min/L^2)	0.0019	0.0064	0.0189	0.0338
	R^2	0.9633	0.979	0.7044	0.7104
	Fitting Equations	y = 0.0019x + 0.0572	y = 0.0064x + 0.0545	y = 0.11x - 2.3509	y = 0.1014x - 2.258

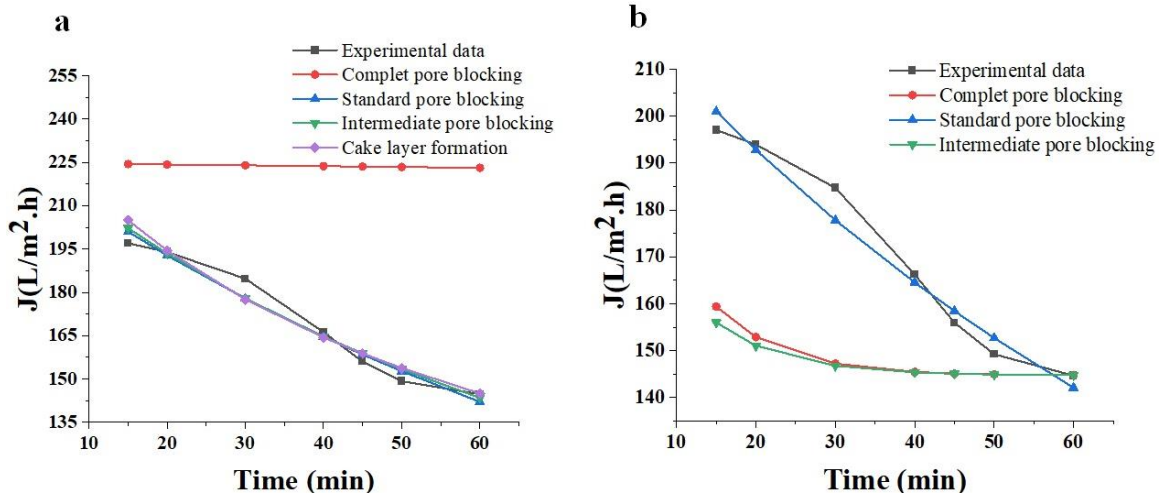

Fig. 10. Comparison of Experimental Data with (a) the Hermia Model and (b) the Filed Model for S3 Membrane

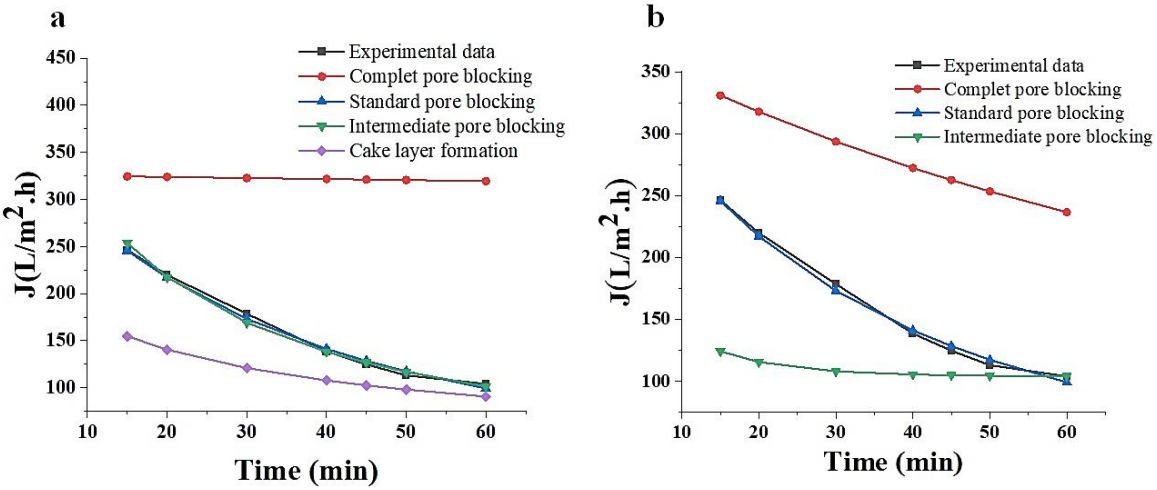

Fig. 11. Comparison of Experimental Data with (a) the Hermia Model and (b) the Filed Model for SN4 Membrane

4.3. Analysis of Variance (ANOVA)

MINITAB-20 software was used to find the response represented by the flux which varied with factors namely time (t), O/W emulsion concentrations (C), temperature (T), and pressure (TMP). The effect of these factors on the flux and oil rejection was studied in previous work [13, 14]. In these studies, the permeate volume was collected during 15 to 60 min and the oil rejection was determined at O/W emulsion concentrations from 100 to 1000 mg/L. The selected best-performed S3 and SN4 membranes which gave the highest flux and oil rejection were tested with a temperature range of 25-45 ^{o}C and TMP of 1.5-3.5 bar. Fig. 12 and Fig. 13 illustrate the 3D response plots for the studied parameters and their effects on the flux decline for S3 and SN4 membranes, respectively. The collected data were statistically analyzed using the surface response methodology (RSM) and central composite design (CCD). It was possible to find the regression equations that explain how the flux changes. It was found that these equations had a high R^2 value of 98.33% for the S3 membrane and 99.52% for the SN4 membrane. The equations correlating the flux with the studied factors are shown in Eq. 14 and Eq. 15:

$$\text{Flux} = 116.9 - 1.349t + 3.56T + 44.4\ \text{TMP} - 0.3307C + 0.01173\ t \times t - 0.0186\ T \times T - 2.08\ \text{TMP} \times \text{TMP} + 0.000127C \times C - 0.0218\ t \times T - 0.260\ t \times \text{TMP} + 0.001100\ t \times C \quad (14)$$

$$\text{Flux} = 304.8 - 7.607t + 1.35T + 17.0\ \text{TMP} - 0.0610C + 0.05346\ t \times t - 0.0141\ T \times T - 1.44\ \text{TMP} \times \text{TMP} - 0.000131C \times C + 0.00274\ t \times T - 0.0231\ t \times \text{TMP} + 0.002461t \times C \quad (15)$$

The regression coefficients of Eq. 14 and Eq. 15 are shown in Table 4 and Table 5 where the P-values were < 0.05 which means that the models are statistically significant.

Table 4. Analysis of Variance for S3 Membrane

Source	DF	Adj SS	Adj MS	F-Value	P-Value
Model	11	226788	20617.1	235.47	0.000
Linear	4	148765	37191.2	424.77	0.000
t (min.)	1	2794	2793.7	31.91	0.000
T (ºC)	1	3173	3172.6	36.24	0.000
TMP (bar)	1	9023	9022.7	103.05	0.000
C. (mg/L)	1	72320	72320.2	825.99	0.000
Square	4	3946	986.6	11.27	0.000
t (min.) *t (min.)	1	297	296.6	3.39	0.007
T (ºC)*T (ºC)	1	17	16.6	19	0.006
TMP (bar)*TMP (bar)	1	21	20.9	24	0.008
C. (mg/L) *C. (mg/L)	1	3099	3099.3	35.40	0.000
2-Way Interaction	3	2822	940.7	10.74	0.000
t (min.) *T (ºC)	1	212	211.6	24.2	0.012
t (min.) *TMP (bar)	1	300	300.0	3.43	0.041
Time (min.) *C. (mg/L)	1	991	991.5	11.32	0.002
Error	44	3852	87.6		
Total	55	230640			

Fig. 14 shows the Perto chart of the standardized effects. Fig. 12 to Fig. 14 show the most affecting factors on the flux, the interaction between these factors, and their effect on the flux. For the S3 membrane, O/W emulsion feed concentration is considered the most important variable that affects the flux value followed by the TMP, temperature, and time. As O/W emulsion concentrations increased the flux declined to about 87.18% due to the deposition of oil drops inside the pores which obstructed the water from passing through the

membrane. Increasing pressure and temperature led to an increase the flux to about 17.25% and 9.62% at the expense of decreasing R% as reported in the previous work [13, 14]. While for SN4, the O/W emulsion feed concentration is considered the most important variable that caused the flux reduction followed by time, TMP, and temperature. Increasing the concentration decreased the flux percent to 60.23%. Increasing temperature and pressure led to an increase in the flux to about 3.43% and 7.65% [13, 14]. The flux reduction with increasing O/W emulsion concentrations and time was due to a large proportion of oil depositing inside the membrane pores and on the surface, causing blockages and reducing the membrane available area for water passage. Therefore, the accumulation of droplets increased as filtration time passed. On the contrary, the flux of S3 and SN4 membranes increased as pressure and temperature increased due to the increase in the force applied on the O/W emulsion by the action of rising pressure so the oil droplets deformed and easily penetrated the membrane pores. Rising O/W emulsion temperature reduced its viscosity which decreased the oil droplet surface tension and facilitated the flow through the membranes.

For both membranes, the interaction between the experiment time and the O/W emulsion concentrations revealed the highest interaction among other variables affecting the flux value. These results support the standard pore-blocking model by Hermia and Field in which the membrane pores are filled with oil droplets during the filtration time causing a flux reduction.

Table 5. Analysis of Variance for SN4 Membrane

Source	DF	Adj SS	Adj MS	F-Value	P-Value
Model	11	198914	18083.1	832.87	0.000
Linear	4	74371	18592.7	856.34	0.000
t (min.)	1	8350	8349.7	384.57	0.000
T (ºC)	1	334	333.9	15.38	0.000
TMP (bar)	1	1222	1221.5	56.26	0.000
C. (mg/L)	1	40441	40441.2	1862.63	0.000
Square	4	9649	2412.3	111.11	0.000
t (min.) *t (min.)	1	6156	6156.5	283.56	0.000
T (ºC)*T (ºC)	1	10	9.5	4.4	0.005
TMP (bar)*TMP (bar)	1	10	9.9	4.6	0.002
C.(mg/L) *C. (mg/L)	1	3305	3304.7	152.21	0.000
2-Way Interaction	3	7033	2344.4	107.98	0.000
t (min.) *T (ºC)	1	3	3.4	15	0.018
t (min.) *TMP (bar)	1	2	2.4	11	0.014
t (min.) *C.(mg/L)	1	4966	4966.3	228.74	0.000
Error	44	955	21.7		
Total	55	199870			

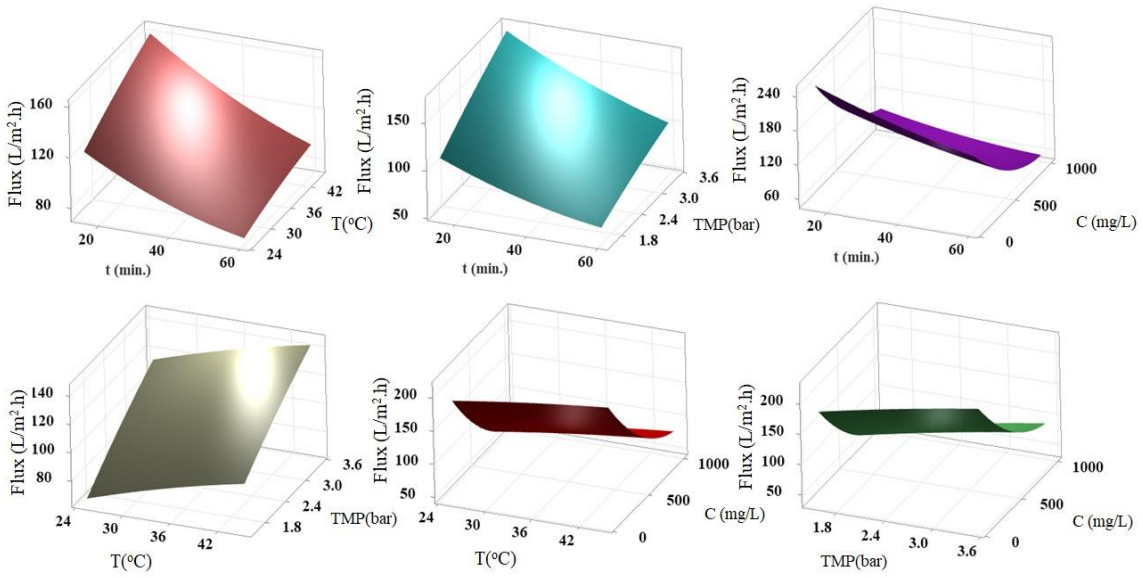

Fig. 12. 3D Response Surface Plots for S3 Membrane

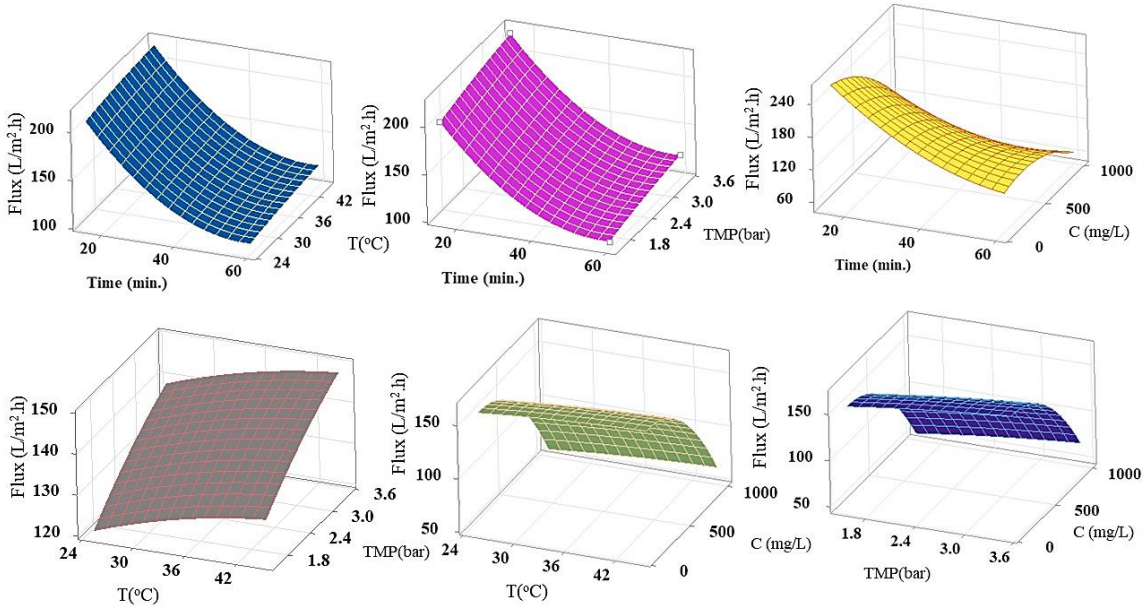

Fig. 13. 3D Response Surface Plots for SN4 Membrane

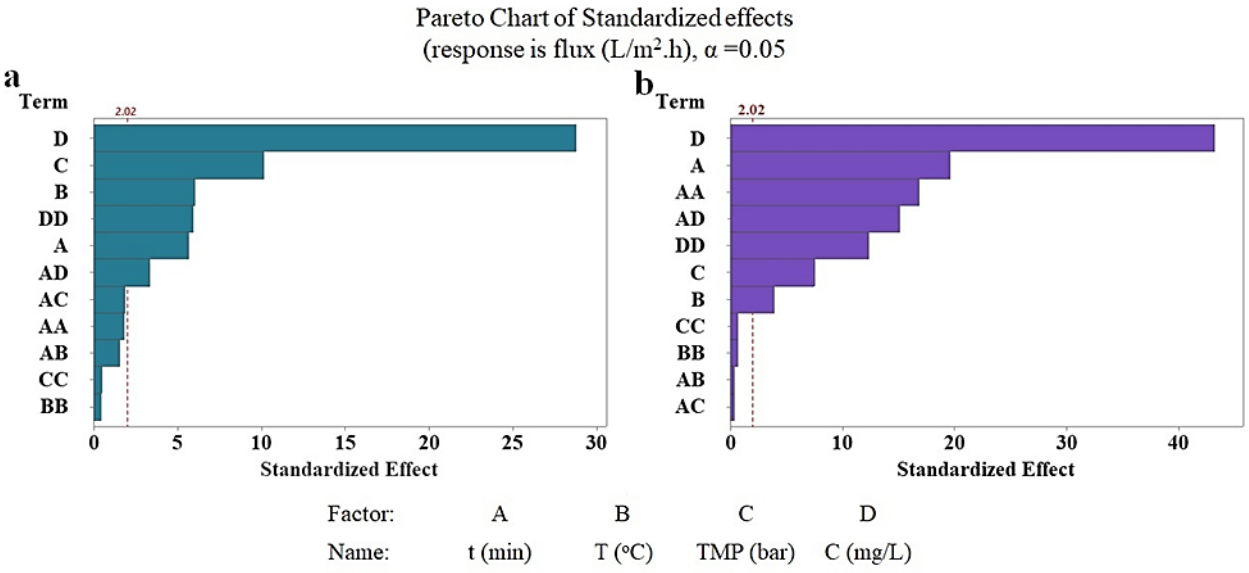

Fig. 14. Perto Chart for (a) S3 Membrane (b) SN4 Membrane

5- Conclusion

The excellent removal efficiency and appropriate flux obtained by the S3 and SN4 MF membranes made them preferable to be used for O/W emulsion separation. The synthesized membranes exhibited high FRR% and low RFR% confirming their promising antifouling during oil separation. The SDS solution showed better performance than the EDTA solution when used as a washing solution to remove oil droplets from both membranes. The R_{ir}% of S3 and SN4 were less than 10% which indicates the effective cleaning procedure that was used in the fouling experiments. The standard pore blocking model successfully explained the fouling occurred in the S3 membrane while the standard pore blocking and intermediate pore blocking using the Hermia model and the modified equations by Field successfully explained the fouling occurred in the SN4 membrane. ANOVA statistics succeeded in obtaining the regression equations which represent the flux of S3 and SN4 membranes with high R^2 of 98.33% and 99.52%, respectively and the flux was highly affected by O/W emulsion feed concentrations. The results of ANOVA support the standard pore-blocking model by Hermia and Field.

References

[1] D. Vasanth, G. Pugazhenthi, and R. Uppaluri, "Cross-flow microfiltration of oil-in-water emulsions using low-cost ceramic membranes," *Desalination*, vol. 320, pp. 86–95, 2013, https://doi.org/10.1016/j.desal.2013.04.018

[2] S. P. A. A. R. Abdel-Aty, Y. S. Abdel Aziz, R. M.G. Ahmed, I. M.A. ElSherbiny and A. S. G. K. M. Ulbricht, "High performance isotropic polyethersulfone membranes for heavy oil-in-water emulsion separation," *Separation and Purification. Technology*, vol. 253, p. 117467, 2020, https://doi.org/10.1016/j.seppur.2020.117467

[3] S. M. Al-Jubouri, S. Al-Batty, R. K. S. Al-Hamd, R. Sims, MW. Hakami, and M. H. SK "Sustainable environment through using porous materials: A review on wastewater treatment," *Asia-Pacific Journal of Chemical Engineering*, vol. 2023; e2941, 2023, https://doi.org/10.1002/apj.2941

[4] H. Rezaei, F. Z. Ashtiani, and A. Fouladitajar, "Fouling behavior and performance of microfiltration membranes for whey treatment in steady and unsteady-state conditions," *Brazilian Journal of Chemical Engineering*, vol. 31, no. 2, p. 503–518, 2014, https://doi.org/10.1590/0104-6632.20140312s00002521

[5] X. Liu, C. Tian, Y. Zhao, W. Xu, D. Dong, K. Shih, T. Yan, and W. Song, "Enhanced cross-flow filtration with flat-sheet ceramic membranes by titanium-based coagulation for membrane fouling control," *Frontiers of Environmental Science and Eng*ineering, vol. 16, no. 8, 2022, https://doi.org/10.1007/s11783-022-1531-x

[6] G. Aysegul, J. Hruza, and F. Yalcinkaya, "Fouling and Chemical Cleaning of Microfiltration Membranes," *Polymers (Basel).*, vol. 13, p. 846, 2021, https://doi.org/10.3390/polym13060846

[7] J. Hermia, "Constant pressure blocking filtration laws. Application to power-law non-Newtonian fluids," *Transactions of the Institution of Chemical Engineers*, vol. 60, p. 183–187, 1982.

[8] R. W. Field, D. Wu, J. A. Howell, and B. B. Gupta, "Critical flux concept for microfiltration fouling," *Journal of Membrane Science*, vol. 100, no. 3, p. 259–272, 1995, https://doi.org/10.1016/0376-7388(94)00265-Z

[9] A. B. Koltuniewicz, R. W. Field, and T. C. Arnot, "Cross-flow and dead-end microfiltration of oily-water emulsion. Part I: Experimental study and analysis of flux decline," *Journal of Membrane Science*, vol. 102, no. C, p. 193–207, 1995, https://doi.org/10.1016/0376-7388(94)00320-X

[10] T. C. Arnot, R. W. Field, and A. B. Koltuniewicz, "Cross-flow and dead-end microfiltration of oily-water emulsions. Part II. Mechanisms and modelling of flux decline," *Journal of Membrane Science*, vol. 169, no. 1, p. 1–15, 2000, https://doi.org/10.1016/S0376-7388(99)00321-X

[11] R. W. Field and J. J. Wu, "Permeate Flux in Ultrafiltration Processes—Understandings and Misunderstandings," *Membranes (Basel).*, vol. 12, no. 2, p. 1–18, 2022, https://doi.org/10.3390/membranes12020187

[12] E. Virga, R. W. Field, P. M. Biesheuvel, and W. M. De Vos, "Theory of oil fouling for microfiltration and ultrafiltration membranes in produced water treatment," *Journal of Colloid Interface Science*, vol. 621, p. 431–439, 2022, https://doi.org/10.1016/j.jcis.2022.04.039

[13] S. A. Sadek and S. M. Al-Jubouri, "Structure and performance of polyvinylchloride microfiltration membranes improved by green silicon oxide nanoparticles for oil-in-water emulsion separation," *Materials Today Sustainability*, vol. 24, no. November, p. 100600, 2023, https://doi.org/10.1016/j.mtsust.2023.100600

[14] S. A. Sadek and S. M. Al-Jubouri, "Highly efficient oil-in-water emulsion separation based on innovative stannic oxide/polyvinylchloride (SnO2/PVC) microfiltration membranes," *Journal of Industrial and Engineering Chemistry*, 2024, https://doi.org/10.1016/j.jiec.2024.06.016

[15] Y. Zhan, X. Chen, A. Sun, H. Jia, Y. Liu, L. Li, Yu. Chiao, X. Yang, and F. Zhu, "Design and assembly of Ag-decorated Bi_2O_3 @ 3D MXene Schottky heterojunction for the highly permeable and multiple-antifouling of fibrous membrane in the purification of complex emulsified oil pollutants," *Journal of Hazardous Materials*, vol. 458, no. May, p. 131965, 2023, https://doi.org/10.1016/j.jhazmat.2023.131965

[16] J. Hu, Y. Zhan, G. Zhang, Q. Feng, W. Yang, Y. Chiao, S. Zhang, and A. Sun, "Durable and super-hydrophilic/underwater super-oleophobic two-dimensional MXene composite lamellar membrane with photocatalytic self-cleaning property for efficient oil/water separation in harsh environments," *Journal of Membrane Science*, vol. 637, no. March, p. 119627, 2021, https://doi.org/10.1016/j.memsci.2021.119627

[17] H. Li, Q. Zhong, Q. Sun, B. Xiang, and J. Li, "Upcycling Waste Pine nut Shell Membrane for Highly Efficient Separation of Crude Oil-in-Water Emulsion," *Langmuir*, vol. 38, no. 11, p. 3493–3500, 2022, https://doi.org/10.1021/acs.langmuir.1c03386

[18] E. S. Awad, T. M. Sabirova, N. A. Tretyakova, Q. F. Alsalhy, A. Figoli, and I. K. Salih, "A Mini-Review of Enhancing Ultrafiltration Membranes (UF) for Wastewater Treatment: Performance and Stability," *Chemengineering.*, vol. 5, p. 34, 2021, https://doi.org/10.3390/chemengineering5030034

[19] C. N. Matindi, M. Hu, S. Kadanyo, Q. V. Ly, N. N. Gumbi, D.S. Dlamini, J. Li, Y. Hu, and Z. Cui, "Tailoring the morphology of polyethersulfone / sulfonated polysulfone ultrafiltration membranes for highly efficient separation of oil-in-water emulsions using TiO_2 nanoparticles," *Journal of Membrane Science*, no. November, p. 118868, 2021, https://doi.org/10.1016/j.memsci.2020.118868

[20] M. R. D. Guzman, C. K. A. Andra, M. B. M. Yap Ang, G. V. C. Dizon, A. R. Caparanga, S. Huang, and K. Lee., "Increased performance and antifouling of mixed-matrix membranes of cellulose acetate with hydrophilic nanoparticles of polydopamine-sulfobetaine methacrylate for oil-water separation," *Journal of Membrane Science*, vol. 620, p. 118881, Feb. 2021, https://doi.org/10.1016/j.memsci.2020.118881

[21] H. N. Alfalahy and S. M. Al-Jubouri, "Preparation and application of polyethersulfone ultrafiltration membrane incorporating NaX zeolite for lead ions removal from aqueous solutions," *Desalinization and Water Treatment*, vol. 248, p. 149–162, 2022, https://doi.org/10.5004/dwt.2022.28072

[22] M. A. and S. Al-Jubouri, "Implementation of hierarchically porous zeolite-polymer membrane for Chromium ions removal Implementation of hierarchically porous zeolite-polymer membrane for Chromium ions removal," *IOP Conference Series: Earth and Environmental Science*, vol. 779, no. 012099, 2021, https://doi.org/10.1088/1755-1315/779/1/012099

[23] W. Hong, C. Li, T. Tang, H. Xu, Y. Yu, G. Liu, F. Wang, C. Leia and H. Zhu, "The photocatalytic activity of the SnO_2/TiO_2/PVDF composite membrane in rhodamine B degradation," *New Journal of Chemistry*, vol. 45, no. 5, p. 2631–2642, 2021, https://doi.org/10.1039/d0nj04764c

[24] F. Costantino, A. Armirotti, R. Carzino, L. Gavioli, A. Athanassiou, and D. Fragouli, "In situ formation of SnO_2 nanoparticles on cellulose acetate fibrous membranes for the photocatalytic degradation of organic dyes," *Journal of Photochemistry and Photobiology A: Chemistry*, vol. 398, no. October 2019, p. 112599, 2020, https://doi.org/10.1016/j.jphotochem.2020.112599

[25] Z. Chen, G. Chen, H.-Yin Xie, Z. Xu, Y. Li, J. Wan, L. Liu, and H. Mao, "Photocatalytic antifouling properties of novel PVDF membranes improved by incorporation of SnO_2-GO nanocomposite for water treatment," *Separation and Purification Technol*ogy, vol. 259, no. September, p. 118184, 2021, https://doi.org/10.1016/j.seppur.2020.118184

[26] A. L. Ahmad, M. A. Majid, and B. S. Ooi, "Functionalized PSf/SiO_2 nanocomposite membrane for oil-in-water emulsion separation," *Desalination*, vol. 268, no. 1–3, p. 266–269, 2011, https://doi.org/10.1016/j.desal.2010.10.017

[27] Z. Yu, X. Liu, F. Zhao, X. Liang, and Y. Tian, "Fabrication of a low-cost nano-SiO_2/PVC composite ultrafiltration membrane and its antifouling performance," *Journal of Applied Polymer Science*, vol. 132, no. 2, 2015, https://doi.org/10.1002/app.41267

[28] I. Veza, M. Spraggon, I. M. R. Fattah, and M. Idris, "Response surface methodology (RSM) for optimizing engine performance and emissions fueled with biofuel: Review of RSM for sustainability energy transition," *Results in Engineering*, vol. 18, no. May, 2023, https://doi.org/10.1016/j.rineng.2023.101213

[29] N. S. A. Yaro, M. H. Sutanto, N. Z. Habib, M. Napiah, A. Usman, and A. Muhammad "Comparison of Response Surface Methodology and Artificial Neural Network approach in predicting the performance and properties of palm oil clinker fine modified asphalt mixtures, Construction and Building Materials," *Construction and Building Materials*, vol. 324, p. 126618, 2022, https://doi.org/10.1016/j.conbuildmat.2022.126618

[30] N. S. Khashi'ie, I. Waini, M. F. Mukhtar, N. A. Zainal, K. B. Hamzah, N. M. Arifin, and I. Pop,"Response Surface Methodology (RSM) on the Hybrid Nanofluid Flow Subject to a Vertical and Permeable Wedge," *Nanomaterials*, vol. 12, no. 22, pp. 1–16, 2022, https://doi.org/10.3390/nano12224016

[31] S. M. Al-Jubouri, "'Preparation of highly-reactive silica from Phragmites (common reed) and using it as an inexpensive silica source to prepare Y Zeolite," 6291, *Patented*, 2020.

[32] S. M. Al-Jubouri, S. I. Al-batty, and S. M. Holmes, "Using the ash of common water reeds as a silica source for producing high purity ZSM-5 zeolite microspheres," *Microporous Mesoporous Materials*, vol. 316, no. October 2020, p. 110953, 2021, https://doi.org/10.1016/j.micromeso.2021.110953

[33] X. Xu, G. Zhang, S. Wang, S. Lv, and X. Zhuang, "Fabrication of fibrous microfiltration membrane by pore filling of nanofibers into poly (ethylene terephthalate) nonwoven scaffold," *Journal of Industrial Textiles*, vol. 50, no. 4, p. 566–583, 2020, https://doi.org/10.1177/1528083719837733

[34] B. Shoba and J. Jeyanthi, "Performance Analysis of Rubber Seed Shell Activated Carbon Incorporated Polymeric Membrane for the Separation of Oil-in-Water Emulsion," *Journal of Polymers and the Environment*, vol. 30, no. 3, p. 1055–1071, 2022, https://doi.org/10.1007/s10924-021-02261-9

[35] S. Emani, R. Uppaluri, and M. K. Purkait, "Cross flow microfiltration of oil-water emulsions using kaolin based low-cost ceramic membranes," *Desalination*, vol. 341, no. 1, p. 61–71, 2014, https://doi.org/10.1016/j.desal.2014.02.030

[36] G. L. D. Pereira, L. Cardozo-Filho, V. Jegatheesan, and R. Guirardello, "Generalization and Expansion of the Hermia Model for a Better Understanding of Membrane Fouling," *Membranes (Basel).*, vol. 13, no. 3, p. 1–21, 2023, https://doi.org/10.3390/membranes13030290

[37] P. Kim, K. Park, H. Gun, and J. Kim, "Comparative analysis of fouling mechanisms of ceramic and polymeric micro-filtration membrane for algae harvesting," *Desalination and Water Treatment*, vol. 173, p. 12–20, 2020, https://doi.org/10.5004/dwt.2020.24697

[38] B. Huang, H. Gu, K. Xiao, F. Qu, H. Yu, and C. Wei, "Fouling Mechanisms Analysis via Combined Fouling Models for Surface Water Ultrafiltration Process," *Membranes*, 10, 149. 2020, https://doi.org/10.3390/membranes10070149

[39] M. C. V. Vela, S. Á. Blanco, J. L. García, and E. B. Rodríguez, "Analysis of membrane pore blocking models adapted to crossflow ultrafiltration in the ultrafiltration of PEG," *Chemical Engineering Journal*, vol. 149, no. 1–3, p. 232–241, 2009, https://doi.org/10.1016/j.cej.2008.10.027

[40] K. Suresh and G. Pugazhenthi, "Cross flow microfiltration of oil-water emulsions using clay based ceramic membrane support and TiO_2 composite membrane," *Egyptian Journal of Petroleum*, vol. 26, no. 3, p. 679–694, 2017, https://doi.org/10.1016/j.ejpe.2016.10.007

[41] H. F. Makki, A. F. Al-Alawy, M. H. Al-Hassani, and Z. W. Rashad, "Membranes Separation Process for Oily Wastewater Treatment," *Journal of Engineering*, vol. 17, no. 2, p. 235–252, 2011, https://doi.org/10.31026/j.eng.2011.02.04

[42] A. F. Al-Alawy and M. K. Al-Ameri, "Treatment of Simulated Oily Wastewater by Ultrafiltration and Nanofiltration Processes," *Iraqi Journal of Chemical and Petroleum Engineering*, vol. 18, no. 1, p. 71–85, 2017, https://doi.org/10.31699/IJCPE.2017.1.6

[43] A. F. Al-alawy, S. Mohsin, and A. Musawi, "Microfiltration Membranes for Separating Oil / Water Emulsion," *Iraqi Journal of Chemical and Petroleum Engineering*, vol. 14, no. 4, p. 53–70, 2013, https://doi.org/10.31699/IJCPE.2013.4.7

[44] M. AAbbasi and A. Taheri, "Modeling of permeation flux decline during oily wastewaters treatment by MF - PAC hybrid process using mullite ceramic membranes," *Indian Journal of Chemical Technol*ogy, vol. 21, no. 1, p. 49–55, 2014, http://nopr.niscpr.res.in/handle/123456789/26250

[45] A. Salahi, T. Mohammadi, M. Abbasi, and F. Rekabdar., "Chemical Cleaning of Ultrafiltration Membrane after Treatment of Oily Wastewater," *Iranian Journal of Chemical Engineering*, vol. 7, no. 3, p. 17–28, 2010.

[46] B. Bolto, J. Zhang, X. Wu, and Z. Xie, "A Review on Current Development of Membranes for Oil Removal from Wastewaters," *Membranes*, vol. 65, no.10, p. 1–18, 2020, https://doi.org/10.3390/membranes10040065

[47] E. Garmsiri, Y. Rasouli, M. Abbasi, and A. A. Izadpanah, "Chemical cleaning of mullite ceramic microfiltration membranes which are fouled during oily wastewater treatment," *Journal Water Process Engineering*, vol. 19, no. March, p. 81–95, 2017, https://doi.org/10.1016/j.jwpe.2017.07.012

[48] N. U. Barambu, M. R. Bilad, M. A. Bustam, K. A. Kurnia, M. H. D. Othman, and N. A. H. M. Nordin, "Development of membrane material for oily wastewater treatment: A review," *Ain Shams Engineering Journal*, vol. 12, no. 2, p. 1361–1374, 2021, https://doi.org/10.1016/j.asej.2020.08.027

[49] F. Kazemi, Y. Jafarzadeh, S. Masoumi, and M. Rostamizadeh, "Oil-in-water emulsion separation by PVC membranes embedded with GO-ZnO nanoparticles," *Journal of Environmental Chemical Engineering*, vol. 9, no. 1, Feb. 2021, https://doi.org/10.1016/j.jece.2020.104992

[50] T. A. A. Geleta, I.V. Maggay, Y. Chang, and A. Venault, "Recent Advances on the Fabrication of Antifouling Phase-Inversion Membranes by Physical Blending Modification Method," *Membranes (Basel).*, vol. 13, p. 58, 2023, https://doi.org/10.3390/membranes13010058

[51] A. Gul, J. Hruza, L. Dvorak, and F. Yalcinkaya, "Chemical Cleaning Process of Polymeric Nanofibrous Membranes," *Polymers (Basel).*, vol. 14, no. 6, 2022, https://doi.org/10.3390/polym14061102

[52] T. Yang, H. Xiong, F. Liu, Q. Yang, B. Xu, and C. Zhan, "Effect of UV/TiO_2 pretreatment on fouling alleviation and mechanisms of fouling development in a cross-flow filtration process using a ceramic UF membrane," *Chemical Engineering Journal*, vol. 358, p. 1583–1593, 2019, https://doi.org/10.1016/j.cej.2018.10.149

[53] A. Rushton, "Mathematical Models and Design Methods in Solid-Liquid Separation.", 1st edition, no. 88. Dordrecht, Netherlands: Martinus Nijhoff Publishers, 1985, https://doi.org/10.1007/978-94-009-5091-7

التحقيق في موديلات التلوث لجسيمات الأكسيد النانوية القائمة على أغشية المصفوفة المختلطة للترشيح الدقيق والمطبقة لفصل مستحلب الزيت في الماء

سارة علي صادق [١]، سما محمد عبد الله [١]، سرحان البطي [٢،*]

١ قسم الهندسة الكيمياوية، كلية الهندسة، جامعة بغداد، بغداد، العراق
٢ قسم تكنولوجيا الهندسة الكيميائية والعمليات، كلية الجبيل الصناعية، مدينة جبيل الصناعية، المملكة العربية السعودية

الخلاصة

يعد تلوث الاغشية مشكلة كبيرة عند استخدام عمليات الترشيح الدقيق لفصل الزيت المستحلب عن الماء. يتضمن هذا العمل تقييم فعالية ازالة مستحلب الزيت في الماء، وتقييم مقاومة القاذورات، ودراسة شكل الغشاء قبل وبعد التلوث والغسيل باستخدام محاليل تنظيف مختلفة بواسطة تحليل المجهر الالكتروني الماسح للانبعاث الميداني. ايضاً، تم تقييم الالية الاساسية المساهمة في انخفاض التدفق في اغشية الترشيح الدقيق اثناء الجريان المتقاطع باستخدام موديلات التلوث مثل موديل هيرميا والموديل المطور بواسطة فيلد. قدمت موديلات حجب المسام القياسية والمتوسطة افضل تنبوء للسلوك التجريبي عند تحليل الانحدار في التدفق مع مرور الوقت لغشاء اكسيد السيلكون الحيوي/ البولي فينييل كلورايد و غشاء اكسيد الستانيك/ البولي فينييل كلورايد. انشأ هذا البحث معادلات انحدار للتدفق لكلا الاغشية حيث ترتبط هذه المعادلات بشكل كبير و بنسبة معامل انحراف معياري ٩٨,٣٣% ل $B\text{–}SiO_2$/PVC و بنسبة معامل انحراف معياري ٩٩,٥٢% ل SnO_2/PVC باستخدام منهجية الاستجابة السطحية. تشير نسبة استرداد التدفق العالية الى تحسن ميزة مقاومة القاذورات على الاغشية المصنعة حيث كانت النسبة ٩٦,٨% بالنسبة ل $B\text{–}SiO_2$/PVC و ٩٤,٦% بالنسبة ل SnO_2/PVC. تتوافق النتائج التي حصل عليها هيرميا وفيلد بشكل جيد مع تحليل منهجية الاستجابة السطحية الذي يدعم الية غلق المسام القياسية.

الكلمات الدالة: اكسيد السلكون الحيوي، البولي فينييل كلورايد، اكسيد الستانيك، موديلات القاذورات، المضادة للقاذورات، الترشيح الدقيق، مستحلب الزيت في الماء.